Available online at www.sciencedirect.com
SCIENCE DIRECT®
Journal of Nuclear Materials 344 (2005) 61–66
journal of nuclear materials
www.elsevier.com/locate/jnucmat

Thermochemical and thermophysical properties of alkaline-earth perovskites

Shinsuke Yamanaka [a,*], Ken Kurosaki [a], Takuji Maekawa [a], Tetsushi Matsuda [b], Shin-ichi Kobayashi [b], Masayoshi Uno [a]

[a] Department of Nuclear Engineering, Graduate School of Engineering, Osaka University, Yamadaoka 2-1, Suita, Osaka 565-0871, Japan
[b] Nuclear Fuel Industries, Ltd., Ohaza-Noda 950, Kumatori-cho, Sennan-gun, Osaka 590-0481, Japan

Abstract

In order to contribute to safety evaluation of high burnup oxide fuels, we studied the thermochemical and thermophysical properties of alkaline-earth perovskites known as oxide inclusions. Polycrystalline samples of alkaline-earth perovskites, $BaUO_3$, $BaZrO_3$, $BaCeO_3$, $BaMoO_3$, $SrTiO_3$, $SrZrO_3$, $SrCeO_3$, $SrMoO_3$, $SrHfO_3$ and $SrRuO_3$, were prepared and the thermal expansion coefficient, melting temperature, elastic moduli, Debye temperature, microhardness, heat capacity, and thermal conductivity were measured. The relationship between some physical properties was studied.

1. Introduction

In an irradiated nuclear fuel, a number of fission product (FP) elements are produced and they affect the fuel performance. Therefore, the behavior of FP elements and the properties of their compounds are very important for evaluation of the fuel safety. It is known that some FP elements are soluble in the fuel matrix and others form the oxide or metallic inclusions [1–6]. The white metallic precipitates composed of Mo–Tc–Ru–Rh–Pd alloys and the oxide precipitates with a perovskite type structure of $(Ba,Sr)(U,Pu,Zr,RE,Mo)O_3$ have been observed in the irradiated oxide fuels. It is considered that the inclusions affect the thermochemical and thermophysical properties of the fuel. On the other hand, the perovskite type oxides have potential to be attractive functional materials, such as thermal barrier coating (TBC) and thermoelectric materials, because they have various unique properties in spite of their relatively simple crystal structure.

We have systematically studied the physical properties of Ba and Sr series perovskites until now [7–12]. The thermochemical and thermophysical properties, viz. the thermal expansion coefficient, melting temperature, elastic modulus, microhardness, heat capacity and thermal conductivity of $BaUO_3$ [7], $BaZrO_3$ [8], $BaCeO_3$ [8], $BaMoO_3$ [9], $SrTiO_3$ [10], $SrZrO_3$ [11], $SrCeO_3$ [11], $SrHfO_3$ [12] and $SrRuO_3$ [12], have been studied. This paper presents a review of the results in references [7–12] in addition to a new result of the physical properties for $SrMoO_3$.

2. Experimental

We prepared polycrystalline samples of the perovskites of $BaUO_3$, $BaZrO_3$, $BaCeO_3$, $SrZrO_3$, $SrCeO_3$,

* Corresponding author. Tel.: +81 6 6879 7904; fax: +81 6 6879 7889.
E-mail address: yamanaka@nucl.eng.osaka-u.ac.jp (S. Yamanaka).

0022-3115/$ - see front matter © 2005 Elsevier B.V. All rights reserved.
doi:10.1016/j.jnucmat.2005.04.017

$SrHfO_3$ and $SrRuO_3$ by mixing the appropriate amounts of MO_2 (M: U, Zr, Ce, Hf and Ru) and $BaCO_3$ or $SrCO_3$ followed by reacting at 1273 K and sintering at 1773 K in a reduction atmosphere. The polycrystalline samples of $BaMoO_3$ or $SrMoO_3$ were prepared by a reduction of $BaMoO_4$ or $SrMoO_4$ under 4% H_2-Ar atmosphere at 1523 K. The polycrystalline sample of $SrTiO_3$ was supplied from Furuuchi chemical Co. Ltd.

The crystal structure of the samples was analyzed with the powder X-ray diffraction method and Raman spectroscopy. The powder X-ray diffraction was performed at room temperature using Cu-Kα radiation. The Raman spectra were recorded with NR-1600 (JASCO Co. Ltd.) using an argon laser with a wavelength of 514 nm operated at 100 mW. In order to determine the chemical composition, the SEM-EDX analysis was performed using HITACHI S-2600H SEM instrument equipped with an energy-dispersive HORIBA EDX-200 system. The oxygen analysis was performed using HORIBA EMGA-550 to identify the oxygen concentration of the samples. For measurements of some physical properties, appropriate shapes of the samples were cut from the sintered pellets. The bulk density was determined by the weight and geometric volume.

In the temperature range from room temperature to about 1000 K, the thermal expansion coefficient was evaluated using a dilatometer under a reducing atmosphere or high temperature X-ray diffraction under helium atmosphere. The melting temperature was measured by a thermal arrest method under a reduction atmosphere.

The longitudinal and shear sound velocities were measured with an ultrasonic pulse-echo method (NIHON MATECH Echometer 1062) at room temperature, which enables us to evaluate the elastic moduli and Debye temperature. From the obtained sound velocities of the sintered pellets with porosity, the elastic moduli and Debye temperature for 100% of the theoretical density were estimated by using a finite element method. Hardness measurements were performed at room temperature using a micro-Vickers hardness tester (MATSUZAWA SEIKI MHT-1). The measurements were repeated ten times for each given sample, and the applied load and loading time were chosen to be 9.8 N and 30 s.

The heat capacity was measured using a differential scanning calorimeter, DSC (ULVAC Co. Ltd.) with triple cells in the temperature range from room temperature to about 1200 K in a high purity argon atmosphere. The samples were heated with small and large temperature intervals. The heat capacity was determined by both enthalpy and scanning methods at individual temperatures. The thermal diffusivity was measured by a laser flash method using ULVAC TC-7000 in the temperature range from room temperature to about 1400 K in vacuum. The thermal conductivity was evaluated from the heat capacity, thermal diffusivity, and density.

3. Results and discussion

From the powder X-ray diffraction patterns and Raman spectra of the samples, it is found that the perovskite type single phase is obtained in the present study. The crystal structure and lattice parameter of the perovskites are summarized in Table 1. The lattice parameters correspond to the reported values [13–16]. The chemical composition of the samples does not deviate from the stoichiometric composition. The O/M ratios of the samples are shown in Table 1.

The conventional parameter describing the geometric distortion of ABO_3 type perovskites is defined as a tolerance factor, t:

$$t = \frac{r_A + r_O}{\sqrt{2}(r_B + r_O)}, \tag{1}$$

where r_A, r_B, r_O are the ionic radii of each atom. The coordination numbers of A and B atoms are 12 and 6, respectively. Ordinarily, the value of 't' is within 0.75–1.1 for the perovskites. The cubic structure has a value near 1. As the value of 't' shifts from 1, a geometric distortion becomes gradually large. The values of tolerance factor of Ba and Sr series perovskites are shown in Table 1. The Shannon's values of the ionic radius [17] are used in the present study.

The thermal expansions of the samples are shown in Fig. 1, together with that of UO_2 [18]. The thermal expansions of Ba and Sr series perovskites nearly equal to that of UO_2, except for $BaMoO_3$, $BaZrO_3$ and $SrHfO_3$. From the slope of the thermal expansion curves shown in Fig. 1, the average linear thermal expansion coefficients α_l at the temperature range were evaluated as shown in Table 1. It is found that $SrHfO_3$ has the highest average linear thermal expansion coefficient ($1.13 \times 10^{-5}\ K^{-1}$).

The melting temperatures T_m measured by the thermal arrest method are shown in Table 1. $SrHfO_3$ shows the highest melting temperature (3200 K). In the present study, the melting temperatures of $BaZrO_3$ and $SrTiO_3$ were not evaluated because of the unclear thermal arrest signal, so the reference values [19,20] are shown in Table 1.

It is empirically confirmed that the linear thermal expansion coefficient varies inversely as the melting temperature for many substances, and for some substances the following relationships between α_l and T_m in K have been reported [21]:

$$\alpha_l \cdot T_m = 0.019 \text{ (for metals)}, \tag{2}$$

$$\alpha_l \cdot T_m = 0.030 \text{ (for fluorite type oxides)}. \tag{3}$$

Table 1
Sample characteristics and physical properties of alkaline-earth perovskites

		$BaUO_3$	$BaZrO_3$	$BaCeO_3$	$BaMoO_3$	$SrTiO_3$	$SrZrO_3$	$SrCeO_3$	$SrMoO_3$	$SrHfO_3$	$SrRuO_3$
Tolerance factor	t	0.935	1.011	0.943	1.047	1.009	0.953	0.889	0.986	0.958	1.001
Crystal system		Cubic	Cubic	Orthorhombic	Cubic	Cubic	Orthorhombic	Orthorhombic	Cubic	Orthorhombic	Orthorhombic
Lattice parameters (nm)	a	0.4404	0.4192	0.8786	0.4040	0.3905	0.5816	0.6126	0.3975	0.5790	0.5569
	b	–	–	0.6251	–	–	0.8225	0.8574	–	0.5851	0.5553
	c	–	–	0.6220	–	–	0.5813	0.6000	–	0.8243	0.7875
Density (%TD)	d	81	89	90	90	99	93	84	89	94	97
O/M ratio		2.96 ± 0.02	3.01 ± 0.01	3.06 ± 0.07	2.97 ± 0.07	–	2.98 ± 0.01	3.00 ± 0.03	2.82	3.03	2.85
Average linear thermal expansion coefficient (K^{-1})	α_l	1.10×10^{-5}	7.13×10^{-6}	1.12×10^{-5}	9.46×10^{-6}	–	9.69×10^{-6}	1.11×10^{-5}	7.98×10^{-6}	1.13×10^{-5}	1.03×10^{-5}
Melting temperature (K)	T_m	2450	2978 [19]	2016	1791	2170 [20]	2883	2266	1967	3200	2575
Shear modulus (GPa)	G	45.8	103	58.7	94.3	99.1	98.5	43.7	69.5	87.9	60.1
Young's modulus (GPa)	E	113	243	154	235	245	269	107	180	220	161
Compressibility (GPa^{-1})	β	0.0138	0.00786	0.00723	0.00648	0.00572	0.00296	0.0156	0.00686	0.00682	0.00583
Debye temperature (K)	θ_D	302	544	394	512	639	591	359	510	490	448
Vickers hardness (GPa)	H_V	5.46	4.95	2.34	3.23	7.77	5.74	2.31	5.48	9.31	12.7
Heat capacity	a	126.6	111.1	115.8	131.8	–	123.2	120.1	121.0	117.9	107.7
($Cp = a + bT + cT^{-2}$)	b	1.61×10^{-2}	1.21×10^{-2}	-1.07×10^{-3}	9.36×10^{-3}	–	6.90×10^{-4}	5.45×10^{-3}	1.19×10^{-2}	1.76×10^{-2}	2.65×10^{-2}
($J\,K^{-1}\,mol^{-1}$)	c	-1.42×10^{6}	-6.22×10^{5}	-1.03×10^{6}	-4.33×10^{6}	–	-2.21×10^{6}	-1.26×10^{6}	-2.73×10^{6}	-8.18×10^{5}	-5.19×10^{5}

The elastic moduli and Debye temperature of $BaUO_3$, $BaZrO_3$, $BaCeO_3$, $BaMoO_3$, $SrTiO_3$, $SrZrO_3$ and $SrCeO_3$ are corrected to the values for 100% of the theoretical density by using a finite element method.

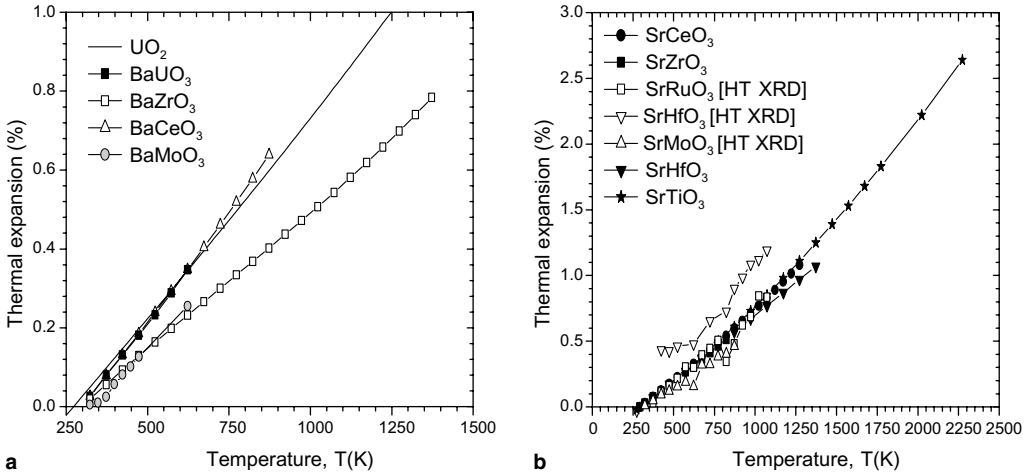

Fig. 1. Thermal expansions of alkaline-earth perovskites: (a) Ba series perovskites, (b) Sr series perovskites.

The relationship between α_l and T_m for the perovskites is shown in Fig. 2, together with the data of other substances [21,22]. Although the products of α_l and T_m for the perovskites have a little scatter, almost the same tendency is observed. The relationship between α_l and T_m for the perovskites is obtained as follows:

$$\alpha_l \cdot T_m = 0.02 \text{ (for perovskites)}. \quad (4)$$

The Vickers microhardness, elastic moduli, and Debye temperature are summarized in Table 1. The elastic moduli and Debye temperature were evaluated from the ultrasonic pulse echo measurements. The elastic moduli and Debye temperature of $BaUO_3$, $BaZrO_3$, $BaCeO_3$, $BaMoO_3$, $SrTiO_3$, $SrZrO_3$ and $SrCeO_3$ are corrected to the values for 100% of the theoretical density by using a finite element method, while those of $SrMoO_3$, $SrHfO_3$ and $SrRuO_3$ are not corrected. It is found that $BaZrO_3$ and $SrZrO_3$ show the highest Young's modulus in Ba and Sr series perovskites, respectively.

It is known that the Debye temperature θ_D can be related to the melting temperature T_m in K, the molar mass M, and the molar volume V_m by the Lindemann relationship [23]. The relationships were reexamined for the perovskites, and the ratio of θ_D to $q^{5/6}(T_m/(MV_m^{2/3}))^{1/2}$ was evaluated to be 1.60 [24], where q is the number of atoms in the chemical formula. Fig. 3 shows this relationship for the perovskites, together with the data of other substances [22,23,25]. The proportionality constants of almost all perovskites are identical (around 1.60), indicating typical characteristics of the

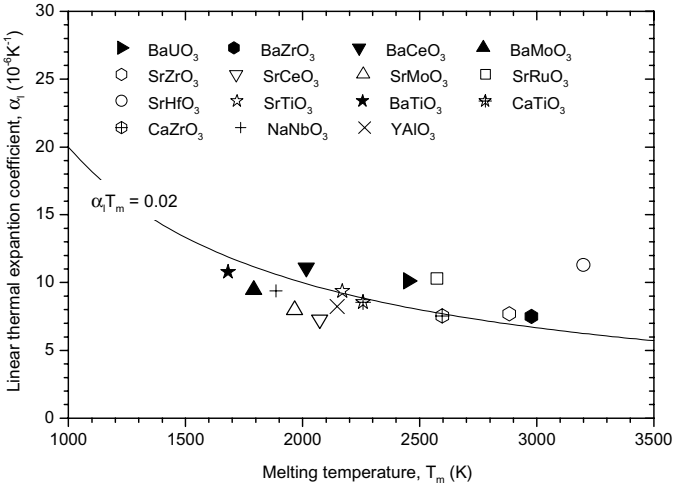

Fig. 2. Relationship between the linear thermal expansion coefficient α_l and melting temperature T_m for alkaline-earth perovskites.

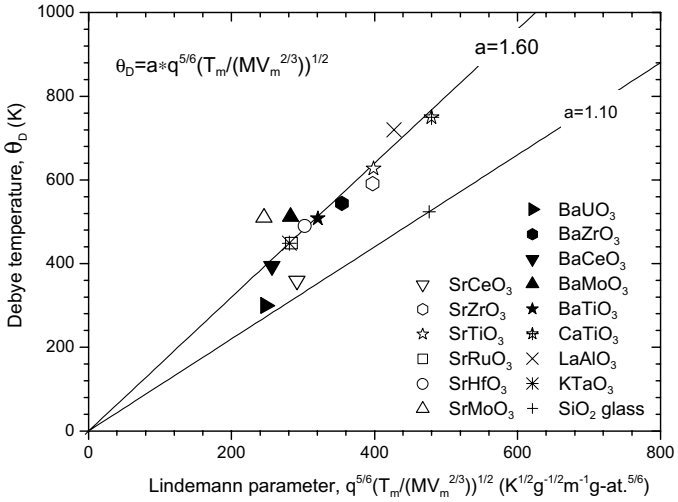

Fig. 3. Relationship between the Debye temperature θ_D and Lindemann parameter $q(T_m/(MV_m^{2/3}))^{1/2}$ for alkaline-earth perovskites.

perovskites. However, the tendency of $BaUO_3$ and $SrCeO_3$ differs from other perovskites, which appears to show the glass-like characteristics.

The heat capacities of the perovskites were measured using triple cells DSC in the temperature range from room temperature to about 1200 K. The empirical equations for heat capacities of the perovskites are summarized in Table 1. Some peaks caused by the phase transitions are observed in the DSC curves of $BaCeO_3$ and $SrZrO_3$. For some of the perovskite type compounds, the heat capacities have been reported previously [19,26]. Our results of the C_P values agree with the literature data [19,26].

The thermal conductivity λ was calculated from the thermal diffusivity D, heat capacity C_P, and density ρ by using the following relationship:

$$\lambda = DC_P\rho. \quad (5)$$

The thermal diffusivity was measured by the laser flash method. The temperature dependence of thermal conductivities of the perovskites is shown in Fig. 4, together with that of UO_2 [27]. The thermal conductivities were corrected to 100% of the theoretical density by using Schulz's equation [28]. The thermal conductivities of the perovskites except for $SrRuO_3$ decrease with increasing temperature, showing that majority of heat

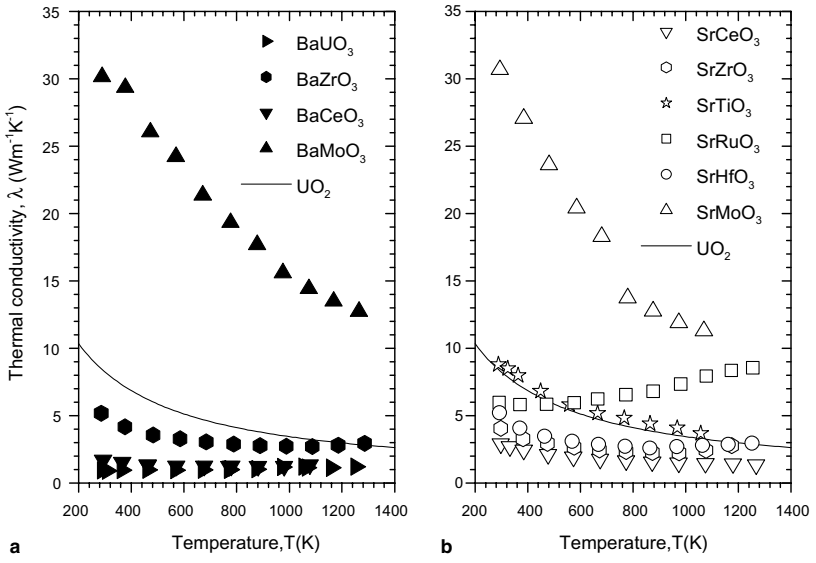

Fig. 4. Temperature dependence of the thermal conductivities of for alkaline-earth perovskites: (a) Ba series perovskites, (b) Sr series perovskites.

conduction carriers are phonons. The thermal conductivity of $SrRuO_3$ increases with increasing temperature, indicating a metallic behavior. The thermal conductivities at room temperature of $BaUO_3$ and $BaCeO_3$ are around 1 $W m^{-1} K^{-1}$, which is about 10 times lower than that of UO_2. On the other hand, $BaMoO_3$ and $SrMoO_3$ show extremely high thermal conductivities, in which the values at room temperature are around 30 $W m^{-1} K^{-1}$. These extremely high thermal conductivities are due to the electronic contributions. We have confirmed very low electrical resistivity of $BaMoO_3$ [9].

The glass-like characteristics of $BaUO_3$ and $SrCeO_3$ are very interesting phenomena, which is not observed for other perovskites. In order to elucidate this characteristic of $BaUO_3$, we have performed the molecular orbital (MO) calculation [29] and semiempirical molecular dynamic (MD) calculation [30]. From the MO calculation, the absolute values of net charges of uranium and oxygen in $BaUO_3$ were found to be much smaller than those of zirconium and oxygen in $BaZrO_3$. From the MD calculation, it was found that the estimated pair potential of U–O is broader and wider than that of Zr–O. These results suggest that the strength of ionic bond of U–O in $BaUO_3$ is much lower than that of Zr–O in $BaZrO_3$. The behavior of uranium ion in the $BaUO_3$ appears to play an important role for the phonon glass characteristics.

4. Summary

The alkaline-earth perovskites, $BaUO_3$, $BaZrO_3$, $BaCeO_3$, $BaMoO_3$, $SrTiO_3$, $SrZrO_3$, $SrCeO_3$, $SrMoO_3$, $SrHfO_3$ and $SrRuO_3$, were prepared and their thermochemical and thermophysical properties were measured. $BaUO_3$ shows extremely low thermal conductivity (<1 $W m^{-1} K^{-1}$) and glass like characteristics in the relationship between several properties. $BaZrO_3$ and $SrZrO_3$ have the highest Young's modulus in the Ba and Sr series perovskites, respectively. The values for $BaZrO_3$ and $SrZrO_3$ are 243 GPa and 269 GPa, respectively. Three peaks correspond to the phase transitions are observed in the DSC curves of $BaCeO_3$ and $SrZrO_3$. The phase transitions of $BaCeO_3$ and $SrZrO_3$ are (orthorhombic–rhombohedral–cubic) and (orthorhombic–tetragonal–cubic), respectively. $BaMoO_3$ and $SrMoO_3$ show extremely high thermal conductivity (>30 $W m^{-1} K^{-1}$). $SrHfO_3$ has the highest melting point (3200 K) and thermal expansion coefficient ($1.13 \times 10^{-5} K^{-1}$).

References

[1] F.T. Ewart, R.G. Taylor, J.M. Horspool, G. James, J. Nucl. Mater. 61 (1976) 254.
[2] H. Kleykamp, J.O. Paschoal, R. Pejsa, F. Thummler, J. Nucl. Mater. 130 (1985) 426.
[3] H. Kleykamp, J. Nucl. Mater. 131 (1985) 221.
[4] D.R. O'boyle, F.L. Browm, A.E. Dwight, J. Nucl. Mater. 35 (1970) 257.
[5] I. Sato, H. Furuya, T. Arima, K. Idemitsu, K. Yamamoto, J. Nucl. Mater. 273 (1999) 239.
[6] I. Sato, H. Furuya, T. Arima, K. Idemitsu, K. Yamamoto, J. Nucl. Sci. Technol. 36 (1999) 775.
[7] S. Yamanaka, K. Kurosaki, T. Matsuda, M. Uno, J. Nucl. Mater. 294 (2001) 99.
[8] S. Yamanaka, M. Fujikane, T. Hamaguchi, H. Muta, T. Oyama, T. Matsuda, S. Kobayashi, K. Kurosaki, J. Alloys Compd. 359 (2003) 109.
[9] K. Kurosaki, T. Oyama, H. Muta, M. Uno, S. Yamanaka, J. Alloys Compd. 372 (2004) 65.
[10] H. Muta, K. Kurosaki, S. Yamanaka, J. Alloys Compd. 368 (2004) 22.
[11] S. Yamanaka, K. Kurosaki, T. Oyama, H. Muta, M. Uno, T. Matsuda, S. Kobayashi, J. Am. Ceram. Soc. 88 (2005) 1496.
[12] S. Yamanaka, T. Maekawa, H. Muta, T. Matsuda, S. Kobayashi, K. Kurosaki, J. Solid State Chem. 177 (2004) 3484.
[13] A.J. Jacobson, B.C. Tofield, B.E.F. Fender, Acta Cryst. B28 (1972) 956.
[14] I. Charrier-Cougoulic, T. Pagnier, G. Lucazeau, J. Solid State Chem. 142 (1999) 220.
[15] K.S. Knight, Solid State Ion. 74 (1994) 109.
[16] K. Kamata, T. Nakamura, T. Sata, Mater. Res. Bull. 10 (1975) 373.
[17] R.D. Shannon, Acta Cryst. A32 (1976) 751.
[18] D.G. Martin, J. Nucl. Mater. 152 (1988) 94.
[19] R. Vassen, X. Cao, F. Tietz, D. Basu, D. Stover, J. Am. Ceram. Soc. 83 (2000) 2023.
[20] N. Sata, H. Matsuta, Y. Akiyama, Y. Chiba, S. Shin, M. Ishigame, Solid State Ionics 97 (1997) 437.
[21] L.G. Van Uitert, H.M. O'Bryan, M.E. Lines, H.J. Guggenheim, G. Zydzik, Mater. Res. Bull. 12 (1977) 261.
[22] Y. Hanajiri, T. Sato, T. Matsui, Netsu Sokutei 26 (1999) 92.
[23] F.A. Lindemann, Physikalische Zeitschrift (14) (1910) 609.
[24] The Chemical Society of Japan ed., Kikan Kagaku Sousetsu, Perovskite-Related Compounds, No. 32, (1997) p. 37.
[25] A. Bartolotta, G. Carini, G. D'Angelo, A. Fontana, F. Rossi, G. Tripodo, J. Non-Cryst. Solids 245 (1999) 9.
[26] E.H.P. Cordfunke, R.J.M. Konings (Eds.), Thermochemical Data for Reactor Materials and Fission Products, North-Holland, Amsterdam, 1990.
[27] MATPRO-Version 11 (Revision 2), NUREG/CR-0497, TREE-1280, August (1981).
[28] B. Schulz, High Temp.–High Pressure 13 (1981) 649.
[29] Y. Kawaharada, H. Kobayashi, K. Kurosaki, M. Uno, S. Yamanaka, H. Nakamatsu, J. Nucl. Sci. Technol. (Suppl. 3) (2002) 784.
[30] K. Kurosaki, T. Oyama, T. Matsuda, M. Uno, S. Yamanaka, J. Nucl. Sci. Technol. (Suppl. 3) (2002) 815.